Resonant inelastic x-ray scattering study of doping and temperature dependence of low-energy excitations in $La_{1-x}Sr_xVO_3$ thin films

Kari Ruotsalainen,[1,2,*] Matteo Gatti,[2,3,1] James M. Ablett,[1] Flora Yakhou-Harris,[4] Jean-Pascal Rueff,[1,5] Adrian David,[6] Wilfrid Prellier,[6] and Alessandro Nicolaou[1,†]

[1]*Synchrotron SOLEIL, L'Orme des Merisiers, Saint-Aubin, Boîte Postale 48, F-91192 Gif-sur-Yvette, France*
[2]*LSI, CNRS, CEA/DRF/IRAMIS, École Polytechnique, Institut Polytechnique de Paris, F-91120 Palaiseau, France*
[3]*European Theoretical Spectroscopy Facility*
[4]*ESRF, 71 avenue des Martyrs, F-38000 Grenoble, France*
[5]*Laboratoire de Chimie Physique, Matière et Rayonnement, Sorbonne Université, CNRS, F-75252 Paris, France*
[6]*Laboratoire CRISMAT, CNRS UMR 6508, ENSICAEN, F-14050 Caen, France*

(Received 8 May 2020; revised 8 April 2021; accepted 21 May 2021; published 24 June 2021)

We present a temperature- and doping-dependent resonant inelastic x-ray scattering experiment at the V $L_{2,3}$ and O K edges in $La_{1-x}Sr_xVO_3$ thin films with $x = 0$ and $x = 0.1$. This material is a canonical example of a compound that exhibits a filling-control metal-insulator transition and undergoes orbital ordering and antiferromagnetic transitions at low temperature. Temperature-dependent measurements at the V L_3 edge reveal an intra-t_{2g} excitation that blueshifts by 40 meV from room temperature to 30 K at a rate that differs between the para- and antiferromagnetic phases. The line shape can be partially explained by a purely local model using crystal field theory calculations. For the low Sr concentration $x = 0.1$, the doping is shown to affect the local electronic structure primarily on the O sites, beyond a simple Mott-Hubbard picture. Furthermore, the presence of phonon overtone features at the O K edge evidences that the low-energy part of the spectrum is dominated by phonon response.

DOI: 10.1103/PhysRevB.103.235158

I. INTRODUCTION

The AVO_3 compounds (A is a rare earth or Y) exhibit antiferromagnetism (AFM) and orbital ordering (OO) at low temperatures [1,2]. In a local picture, the V atoms have a d^2 configuration in a slightly compressed octahedral local environment. Physical understanding of the AFM/OO in AVO_3 relies on two views: the ordering transitions are associated with the Jahn-Teller effect or orbital superexchange between nearly degenerate nearest-neighbor vanadium t_{2g} electronic states [3–16]. The splitting of the t_{2g} states as a function of temperature and doping is an important parameter for elucidating the physical drivers of the phase transitions. The strength of the orbital superexchange is dependent on the V-O-V bond angles connecting adjacent octahedra. For bulk YVO_3 (YVO) the V-O-V angles remain below 145° between room temperature and 65 K, and it was concluded that crystal field splitting is the dominating factor [17–19]. Bulk $LaVO_3$ (LVO) exhibits V-O-V angles within a range of 156° to 158° in the same temperature range [20]. Strained epitaxial LVO is a particularly interesting case [21–26] for further study as the structure is modified by the epitaxial growth constraints, and the V-O-V angles straighten to 164°–168° [27].

Bulk LVO is a paramagnetic (PM) insulator at room temperature [28,29]. The AFM and OO transitions are found near $T = 140$ K in single crystals [2,15,29–31]. The room temperature crystal structure of LVO is orthorhombic (*Pnma*), and it distorts to a monoclinic structure ($P2_1/a$) upon entering the AFM/OO state [8,20,32]. The structure of epitaxial LVO films grown on the (001) surface of $SrTiO_3$ (STO) has been studied with diffraction methods that found the structure can be refined assuming either *Pnma* or $P2_1/m$ space groups [27,33,34]. Temperature-dependent diffraction studies give no indication of a structural phase transition breaking the lattice symmetry [35,36]. The AFM transition in epitaxial films is, however, seen in temperature-dependent magnetization measurements on LVO and in the related compound $PrVO_3$ [37]. The occurrence of the OO transition in LVO on STO was deduced from Raman spectroscopy [38–40]. Recent investigations of strained LVO films by low-energy muon spin spectroscopy and ellipsometry measurements showed that the compressive strain reduces by only a few kelvin the OO and AFM transition temperatures and does not suppress the bulk G-type orbital order [41].

$La_{1-x}Sr_xVO_3$ (LSVO) is considered a paradigmatic compound exhibiting a filling-control metal-insulator transition [42–44]. In LVO a 1.0 ± 0.2 eV band gap opens between V t_{2g} states, while V e_g states are completely empty [45]. Within the Zaanen-Sawatzky-Allen classification [46], LVO belongs to the Mott-Hubbard regime [44]. Sr doping induces a metal-insulator transition in $La_{1-x}Sr_xVO_3$ at $x = 0.17$ and also reduces the AFM and OO critical temperatures and ultimately suppresses the transitions at $x = 0.27$ [28,29,43,47,48]. In a pure Mott-Hubbard picture, Sr substitution leads to hole

*kari.ruotsalainen@helmholtz-berlin.de
†alessandro.nicolaou@synchrotron-soleil.fr

doping, converting V^{3+} ions into V^{4+} (i.e., passing from a $3d^2$ to a $3d^1$ electronic configuration). Core-level photoemission experiments on $La_{1-x}Sr_xVO_3$ have shown that the fraction of V^{4+} with respect to V^{3+} is, indeed, enhanced upon hole doping at a high Sr concentration of $x = 0.4$ [35]. Since the Sr^{2+} ions have larger radii than La^{3+}, the structure (un)distorts towards the cubic structure of $SrVO_3$, and the bandwidth also increases [43,44]. Sr doping is expected to form an empty band of acceptor states near the Fermi level, which is progressively broadened with increasing doping until it overlaps with the filled t_{2g} band, giving rise to a metal [49].

The electronic low-energy excitation spectrum of LVO has been characterized with optical spectroscopies [28,48,50–52], in which the crystal field transitions are weak because they are forbidden by the dipole selection rules. Resonant inelastic x-ray scattering (RIXS), on the other hand, excels at revealing crystal field transitions at L absorption thresholds of $3d$ transition metal atoms [53]. Recent advances [54] in energy resolution have made detailed studies of low-energy crystal field splittings even well below 100 meV possible [55,56]. Low-energy excitations were clearly resolved in YVO employing RIXS at ≈60 meV resolution [18]. This experiment focused on the dispersion of the low-energy excitations across the phase diagram. Bulk LVO [57] and $NdVO_3$ [58] have been studied with RIXS at 0.4 eV resolution. Due to the modest energy resolution the line shapes of low-energy excitations could not be resolved.

In this paper we present a RIXS study of the temperature and doping dependencies of low-energy excitations in $La_{1-x}Sr_xVO_3$ thin films with $x = 0$ and $x = 0.1$ (LSVO). We analyze the effects of doping by comparing the V L and O K edge absorption and RIXS spectra recorded at moderate energy resolution. We find that the light Sr doping does not cause clear signatures of V^{4+} ions, but rather affects the local electronic structure on the O site. Furthermore, using measurements with state-of-the-art energy resolution, we show further that the intra-t_{2g} excitations in LVO blueshift by 40 meV when cooling from room temperature to 30 K and that the rate of the blueshift changes between the PM and AFM phases.

II. EXPERIMENTAL METHODS

LVO and LSVO thin films were grown on STO (001) substrates using the pulsed laser deposition (PLD) method. A KrF excimer laser ($\lambda = 248$ nm) with a repetition rate of 2 Hz and laser fluence of ≈2 J/cm^2 was focused on stoichiometric ceramic targets. All the films used in this study were deposited at an optimum growth temperature of 920 K and under oxygen partial pressure of 10^{-6} mbar. PLD yields high-quality epitaxial films of LVO, as shown by structural, transport, and optical studies [27,33,38]. We show the $P2_1/m$ structure of LVO on STO alongside with the scattering geometry in Fig. 1. The substrate plane normal is along the [101] direction of the LVO crystal structure, and the film has a domain structure characterized by fourfold rotations about the plane normal [33]. In terms of the V-O bonds, this means that long and short V-O bonds alternate along the surface of the sample. We performed the x-ray absorption (XAS) measurements using circular left (CL) polarized light. The XAS and the RIXS spectra discussed later are considered averages over the appropriate incident and outgoing polarization states. RIXS experiments were performed at both V $L_{2,3}$ and O K edges using CL and linear-vertical (LV) polarized light. Several sets of measurements on different samples having the same doping were performed at the SEXTANTS beamline [59] of the Synchrotron SOLEIL using the AERHA (Adjustable Energy Resolution High Acceptance) spectrometer [60]. These measurements, performed with an overall energy resolution ranging from 100 to 180 meV (FWHM), were used to check the reproducibility of the experimental results and to discover the temperature effect on the low-energy losses measured at the V L_3 edge. Once the reproducibility and the robustness of the results were proven, high-resolution measurements were carried out at the ID32 beamline of the European Synchrotron Radiation Facility using the ERIXS spectrometer [54]. The overall experimental resolution of approximately 40 meV allowed us to track precisely the temperature behavior of the energy loss peaks of interest. The XAS spectra presented in this paper were recorded during the experiments at SOLEIL using total fluorescence yield (TFY) detection. The probing depths of TFY and RIXS are of the order 100 nm. The former is more sensitive to the sample surface region as low-energy fluorescence (e.g., V M shell, La N shell) is also detected.

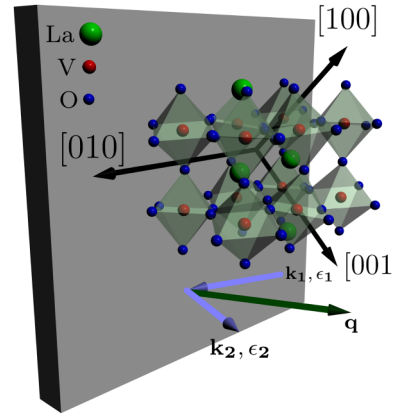

FIG. 1. The crystal structure of strained LVO drawn from a refined $P21/m$ structure [27] together with the experimental scattering geometry. Incident light defined by the photon energy $\hbar\omega_1$, wave vector $\vec{k}_1$, and polarization vector $\vec{\epsilon}_1$ is scattered to a state defined by $\hbar\omega_2$, $\vec{k}_2$, and $\vec{\epsilon}_2$, transferring energy $\hbar\omega = \hbar\omega_1 - \hbar\omega_2$ and momentum $\hbar\vec{q} = \hbar\mathbf{k}_1 - \hbar\mathbf{k}_2$. $\mathbf{k}_1$ makes an angle of 20° with the sample surface plane, and the scattering angle is 85°.

III. RESULTS AND DISCUSSION

A. Hole doping of $La_{1-x}Sr_xVO_3$: Comparing V L and O K edge XAS and RIXS

In this section we discuss the evolution of the electronic structure upon doping by comparing the XAS and RIXS measurements for LVO and LSVO. XAS at the V $L_{2,3}$ edge is shown in Fig. 2(a), and the O K edge region is presented in Fig. 2(b). In Fig. 2(c) we present RIXS data acquired at

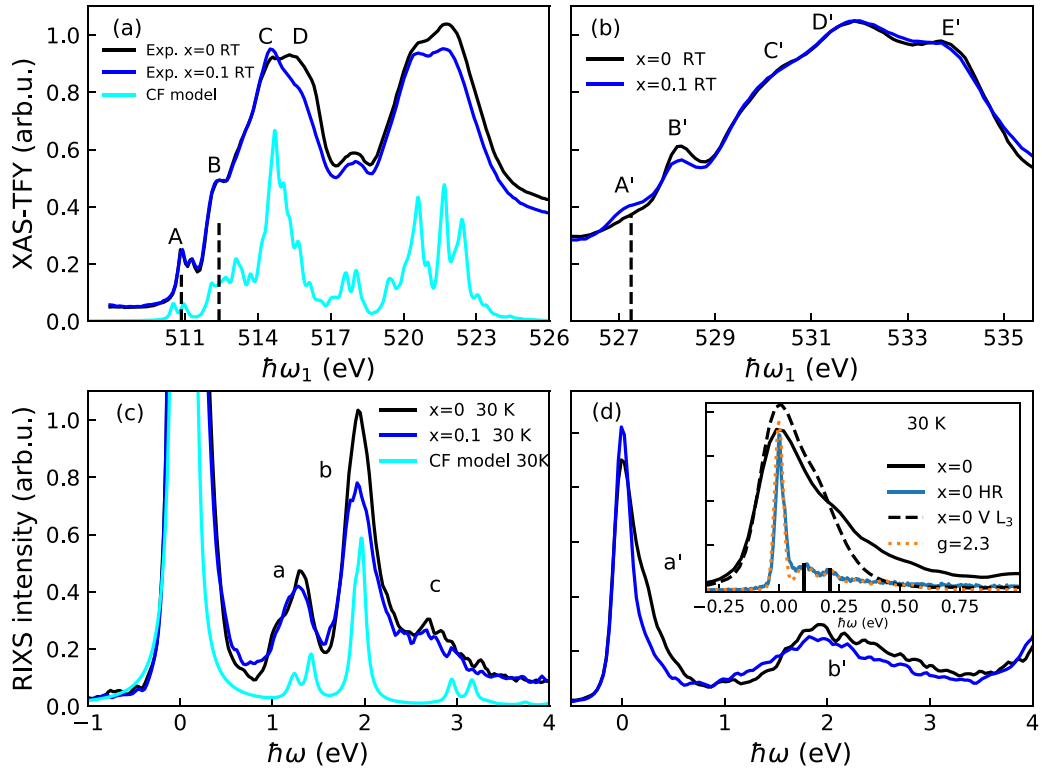

FIG. 2. (a) Comparison of XAS-TFY spectra for LVO and LSVO measured at room temperature (RT) using CL polarized light at the V L edges and a crystal field model (CF). Constant backgrounds were subtracted, followed by normalization to the first prepeak of the V L_3 edges (feature A). (b) The O K edge region. The spectra are normalized to D'. (c) Low-temperature RIXS spectra recorded at feature B of (a). The spectra were processed by subtracting constant backgrounds and normalizing to the maximum of feature b of the $x = 0$ spectrum. The CF model calculation is scaled for presentability. (d) Low-temperature O K edge RIXS spectra excited at feature A′ of (b). In the inset we compare low-energy excitations observed at the V L_3 edge with the ones observed at the preedge region of the O K edge. Furthermore, the high resolution (HR) O K edge RIXS spectrum showing phonon excitations is well reproduced by the Ament model [61] using a phonon energy of 105 meV and an electron-phonon coupling constant $g = 2.3$.

the V L_3 edge exciting on B (512.4 eV). Finally, in Fig. 2(d) we show RIXS spectra obtained at the O K edge by exciting on A′ (527.3 eV), where in the intermediate state an O 1s core electron is promoted to a hybridized O $2p$/V t_{2g} state.

Comparing the XAS measurements in Figs. 2(a) and 2(b), we note that while the line shape of the low-energy part of the V L_3 edge (A, B) remains unchanged upon 10% Sr to La substitution, the preedge region (A′ and B′) of the O K edge is strongly modified.

To understand how the hole doping affects the spectra and the electronic structure of LVO, we first analyze the character of the main features in the XAS spectra, and we describe what is expected from the appearance of a d^1 contribution at the V L_3 edge. The V L_3 XAS in a d^2 configuration and a quasi-O_h crystal field is characterized by a double prepeak structure with maxima located at 510.8 and 511.2 eV (A), a shoulder at 512.4 eV (B), and a main peak at 514.6 eV (C). All these features have been found in the XAS spectra of several vanadates, including bulk LVO [57], hybrid molecular beam epitaxy [62] and pulsed laser deposition [63] grown films, bulk YVO [18,64], and bulk $NdVO_3$ [58]. The line shapes of AVO_3 are essentially the same as in V_2O_3 [65]. Instead, in a $3d^1$ configuration the double prepeak feature A is absent [66], and the line shape is dominated by a shoulder and a main peak that are found at higher energies [64–67]. The shoulder feature of d^1 overlaps with the high-energy peak of A, and hence, the intensity ratio of the peaks at A should change with the introduction of d^1. As noted in the second paragraph of this section, the spectra overlie one another from A to almost up to C. Therefore, the line shape of the V L_3 XAS gives us no indication of d^1. This interpretation will receive further support from the RIXS results discussed later.

Above C at 516 eV [D in Fig. 2(a)], the XAS spectra of LVO and LSVO start to deviate. We attribute this discrepancy to surface contamination. Photoemission experiments have, indeed, shown that the near-surface layers of upcapped LVO films contain V^{4+} and that their concentration is enhanced over time [68]. Furthermore, we note that XAS measurements on YVO report a C/D ratio that evolves with temperature, but the authors did not emphasize this behavior [18]. We can therefore conclude that the XAS spectra representative of the bulk electronic structure of LVO and LSVO films remain unchanged at the V L_3 edge upon light hole doping, at odds with our observations at the O K edge.

In order to compare O K edge XAS spectra of LVO and LSVO we have normalized them by imposing the same intensity at D′. We used a different normalization factor with respect to the one used for the V L_{23} edges in order to highlight

the relative variations occurring in the preedge region (A′, B′). The evolution of the O K edge spectra as a function of hole doping would, indeed, be less visible by using a unique normalization factor for V and O edges. The deviation of the XAS spectra at V L_{23} edges for energies above C is related to a different background originating from the different spectral weight present at D and affecting also the baseline before the O K edge. Therefore, our interpretation relies on only the differences observed in the XAS line shapes. We do not compare O with respect to V intensities or draw any conclusion based on the absolute intensities of the XAS features.

The O K edge XAS spectra are characterized by two preedge peaks, A′ and B′, at 527.3 and 528.2 eV, followed by structures C′ at 530.3 eV, D′ at 531.9 eV, and E′ at 533.8 eV. Prepeaks A′ and B′ have been assigned to exchange-split V t_{2g} states hybridized with O $2p$, and peaks C′ and D′ have been assigned to the e_g states hybridized with O $2p$ [69]. Local density approximation (LDA) + Hubbard U calculations have also been used to assign features A′ and B′ similarly, C′ to O $2p$ hybridized with e_g states, and D′ and E′ to La $5d$ states hybridized with O $2p$ [57]. Isoelectronic Lu doping was experimentally studied, and the experimental XAS results show no significant changes in intensity at the O K preedges even for pristine $LuVO_3$ [57]. Therefore, the changes observed at A′ and B′ reveal the introduction of holes in the valence band. Hence, at least up to 10% Sr replacement the doping does not seem to affect the V site electronic structure by a change in valency, but rather indirectly via the O orbitals that are hybridized with the t_{2g} states of vanadium. Our results thus reveal a deviation from pure Mott-Hubbard like behavior. This conclusion is consistent with interpretation of photoemission and electron energy loss data on LSVO [49]. Similar behavior at light doping is also found in $Y_{1-x}Ca_xVO_3$ [64]. Cuprates and NiO, i.e., late transition metal oxides belonging to a different class of charge transfer insulators, also behave similarly [70,71]. This suggests that a rigid classification into Mott-Hubbard or charge-transfer compounds can be an oversimplification for the rich physics of the doping of transition-metal oxides.

The absence of V d^1 states upon light doping is further confirmed by our RIXS measurements presented in Fig. 2(c). The crystal field excitations are labeled a–c. Peak a at 1.2 eV is a $\Delta S = 1$ intra-t_{2g} transition with the low- (high-) energy edge representing final states with 1 (2) electrons occupying the upper t_{2g} states. Peak b at 2 eV corresponds to $S = 1$ final states with an electron transferred across the e_g-t_{2g} crystal field gap. Excitations a and b reflect Hund's exchange and the octahedral component of the crystal splitting between the t_{2g} and e_g states, respectively [72,73]. Feature c at 2.7 eV consists of higher-energy terms with an excitation across the crystal field gap and a high-energy $\Delta S = 1$ intra-t_{2g} transition. These assignments were made using crystal field calculations (Sec. III D) and are in agreement with previous analyses [18,57,58]. They are also consistent with a quantum chemistry calculation for VOCl (d^2) [74]. Considering that peak a is absent for a d^1 system (see, e.g., $LaTiO_3$ [75]), if some of the holes are localized on V sites, the intensity of peak a can only decrease. For peak b one expects the intensity to increase due to the d^1 component. The ratio of peak a area to peak b area is hence expected to be reduced. In our data the ratio is, in fact, enhanced, excluding the presence of V d^1 sites. This can be understood by considering the influence of the rare-earth atom on the V-O hybridization. Chemical bonding in $3d^1$ rare-earth vanadates and titanates has been studied with LDA + dynamical mean field theory (DMFT) and has shown that the rare-earth-atom states form σ bonds with the same oxygen orbital that forms π bonds with the metal t_{2g} [76]. Furthermore, the Sr contribution to the t_{2g} states is lower in $SrVO_3$ than the La contribution in $LaVO_3$ [77]. The final states corresponding to peak b have an occupied e_g orbital and hybridize stronger with the neighboring O atoms than t_{2g}-type states. According to LDA+U calculations [57] the unoccupied e_g states overlap in energy with the La $5d$ states. Therefore, the intensity reduction seen particularly for peak a and to some extent b are explained the evolution of the hybridization in the RIXS final states.

B. Phonon and electronic excitations at the O K edge

In this section we discuss in detail the low-energy excitation spectrum measured at the O K edge. Low-energy excitations are observed in an overlapping energy range below 1 eV at both the V and O edges when the excitation energy is tuned over states with t_{2g} character [see the inset in Fig. 2(d)]. In order to discuss the origin of these excitations, we track their evolution with doping, and we employ state-of-the-art energy resolution to resolve their components. Our results point toward a phonon origin of the low-energy excitations showing up at the O K edge, hence having a different nature with respect to the ones observed at the V L_3 edge, which have an orbital origin.

In the main panel of Fig. 2(d) we compare RIXS spectra of LVO and LSVO. They were acquired at 30 K with an excitation energy of 527.3 eV [A′ in Fig. 2(b)]. In LVO we observe a shoulder near the elastic line, labeled a′. This feature, which extends up to 0.7 eV, is strongly reduced in LSVO. This means that such an excitation is dramatically affected by Sr to La substitution. This observation marks a clear difference with respect to the low-energy excitations we observed at the V L_3 edge, which appear very similar in LVO and LSVO [Figs. 3(a)–3(c)]. Another important dissimilarity is revealed by the high-resolution data of LVO presented in the inset of Fig. 2(d). They allow us to clearly resolve peaks at 105 and 210 meV at the O K edge. Their constant energy spacing together with the small FWHM points to a phonon origin. Orbital excitation continua are, indeed, expected to be much broader in energy, consistent with our observations at the V L_3 edge. The high-resolution spectrum, which was acquired by using an excitation energy detuned by 500 meV with respect to A′, can be well described by the Ament model [see Eq. (3) of Ref. [61]]. This simple model accounts for the coupling of the excited electron with a single nondispersive phonon. A satisfactory representation of the experimental spectrum is obtained with an electron-phonon (el-ph) coupling constant $g = 2.3$ and a phonon energy of 105 meV. Considering the possibility of multiphonon excitations and the phonon dispersion at finite momentum $\mathbf{q}$, the value of 105 meV match well with phonons involving oxygen octahedra, whose energies are as large as 90 meV at $\mathbf{q} = 0$ as deduced from Raman spectroscopy [39,40]. We think that, while the phonon origin

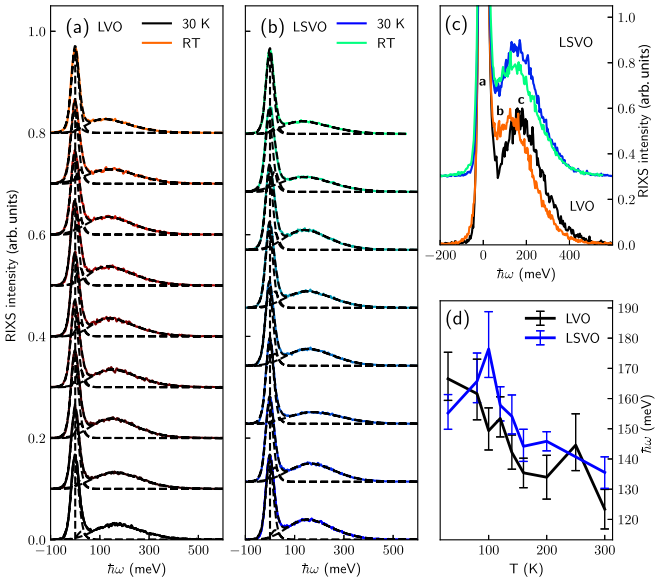

FIG. 3. Temperature-dependent high-resolution RIXS with 40 meV overall resolution. The presented spectra were measured with the incident photon energy tuned to feature A of Fig. 2(a). (a) The temperature-dependent RIXS spectra for $x = 0$. The spectra are normalized to their maxima, and they are ordered by increasing temperature. (b) The temperature series for $x = 0.1$. (c) The end point temperature RIXS spectra for $x = 0$ and $x = 0.1$. The color coding is as in (a) and (b). Different regions in the spectra are marked with the bold letters: **a** corresponds to the elastic line, **b** corresponds to the energy region from approximately 30 to 100 meV, and **c** corresponds to the clearly resolved peak near 150 meV. (d) The extracted temperature dependence of peak **c** for $x = 0$ and $x = 0.1$. The fitting model is explained in the text.

of such a low-energy excitation showing up at the O K edge is certain, the extraction of a reliable el-ph coupling constant is not straightforward due to the complex process through which phonons are excited during the RIXS process. The deviations with respect to the Ament model can be explained considering two effects. The neglect of mode coupling [78,79] is probably a significant reason, as perovskite oxides have several close-lying high-energy optical branches [80]. The distortion of the intermediate-state potential energy surface due to the intermediate-state core exciton also affects the phonon intensities [79]. That said, a full understanding of the phonon spectrum of LVO, including the identification of the phonon modes involved together with precise determination of the el-ph coupling constant, would require a dedicated study including several excitation energies and experimental geometries, which is beyond the scope of the present work.

In a previous RIXS study on YVO [18] the low-energy excitations at the O K edge were interpreted as single and double orbital excitations. Our data point toward a different scenario. The clear presence of phonon progression suggests that a′ exhibits dominant phonon contributions. The long tail toward higher-energy losses would be related to multiple phonon excitations in response to core excitation [81]. Moreover, our interpretation accounts for the strong suppression of a′ by light doping as well, which would be due to disorder-induced reduction of phonon lifetimes with the consequent broadening. This is consistent with Raman scattering results for Ca doping of YVO, where 2% Ca replacement causes a significant broadening of the phonon excitations [82].

It is interesting to remark that O K edge RIXS in molecular liquids features a long extending continuum of excitations when excited at O K preedge resonances [78,81,83]. Hence, a dielectric environment does not suppress the vibrational RIXS signal with respect to the gas phase [84]. Moreover, several well-resolved vibration harmonics were observed by RIXS at the N K edge in the k-(BEDT-TTF)$_2$Cu$_2$(CN)$_3$ charge transfer salt (bis-ethylenedithio-tetrathiafulvalene) [85]. Considering long-range ordered oxides with 3d or lighter metal atoms, RIXS on the O K edge has been studied for, e.g., Li_2CuO_2 and $GeCuO_3$ [86], $Al_2Si_2O_5(OH)_4$ [87], and $SrTiO_3$ [88], i.e., in systems very different in their electronic structure and magnetic properties, yet continuum features extending past 0.5 eV energy losses are found.

The O K edge RIXS presented in Fig. 2(d) reveals an additional feature labeled b′, which is broad and centered at about 2 eV energy loss. This feature, which is also present in YVO, was attributed to excitations between the lower and upper Hubbard bands [18]. It was also noted that the onset energy of b′ in YVO matches rather well with the onset of optical conductivity for YVO [18]. Consistent with our data, showing the presence of more spectral weight at lower-energy loss in LSVO, the onset of the optical conductivity of LSVO is found well below that of LVO [82]. Doping-induced disorder effects on the density of states of AVO_3 compounds in the vicinity of the band gap have been studied using a multiband Hubbard model Hamiltonian approach [89]. They show defect-induced unoccupied states appearing just below the upper Hubbard band, which is likely at the origin of the evolution presented here.

C. Temperature dependence of RIXS at the V L_3 preedge

In this section we focus on the intra-t_{2g} excitations, which are found below 200 meV energy loss. They are best resolved when exciting the system at feature A of Fig. 2(a) [see the inset of Fig. 2(d)].

To get more insight concerning these low-energy excitations and to relate them to the phase diagram of the AVO_3 vanadates, we acquired high-resolution data as a function of temperature from 30 K to room temperature. We have used the state-of-the-art energy resolution of 40 meV. Data for LVO and LSVO are presented in Figs. 3(a)–3(b), respectively. Figure 3(c) displays a comparison between LVO and LSVO at the end points of the temperature series (30 and 300 K). Near the elastic line (labeled **a**) we reveal the presence of an asymmetric peak (**c**) which has a maximum in the 140–160 meV range and a long tail that reaches the baseline near 500 meV. Furthermore, there are temperature-dependent intensity variations in the 30–80 meV energy range. We label this energy region **b**. The complex temperature evolution we found reveals that different contributions are present with possibly differing temperature dependencies.

In order to track the temperature evolution of feature **b** we have used a fitting model that we briefly describe here. Inelastic neutron scattering and Raman scattering studies show that magnon and phonon modes are expected in the **b**

region [31,39,90]. Hence, we use resolution-limited Pearson VII functions to capture **a** and **b** and a skewed Gaussian function to represent **c**. We tested for the necessity of introducing a peak for **b** by trying to reproduce the temperature evolution of peak **c** by a simple blueshifting, using its line shape at 30 K, but we could not obtain a satisfactory fit, indicating that our data are not consistent with a single blueshifting asymmetric peak. Therefore, a peak at **b** is necessary for the fit, and we assume that there are unresolved and/or intrinsically broad excitations contributing to the spectrum and to the line shape of **c** with temperature. We allowed the **b** peak energy loss to vary in the range of 20–50 meV in the final results. All parameters of the skewed Gaussian component were allowed to vary.

The temperature dependence of the maximum of **c** is presented in Fig. 3(d). We can identify two distinct regions in the temperature behavior. From 300 to 140 K the position of the maximum of **c** can be considered temperature independent within the error bars for both compounds. At lower temperatures, the maximum starts to blueshift. For LSVO the energy loss reaches a maximum at 100 K, while for LVO **c** continues to blueshift down to the minimum temperature of 30 K. It is interesting to remark that in $La_{1-x}Sr_xVO_3$ single crystals 140 and 100 K are the temperatures where both magnetic and structural transitions occur in LVO and LSVO, respectively. Ellipsometry measurements show that the OO is maintained in strained LVO/STO films and it occurs at $T_{OO} = 135$ K. That said, pinpointing the origin of the difference in the T evolution between LVO and LSVO would benefit from a more thorough understanding of the magnetic and structural properties of strained films as a function of Sr to La substitution. We will discuss the origin of this temperature behavior in Sec. III E in light of the crystal field calculations presented in Sec. III D.

A high-resolution RIXS study of YVO also observed low-energy excitations at 100–200 meV [18]. Consistent with our data, an overall shift of 30–40 meV between room temperature and 30 K was observed [18]. For $NdVO_3$ [58] a temperature-dependent peak was observed at 400 meV energy loss when exciting the RIXS near the maximum of the V L_3 absorption into dominantly e_g symmetry states, and it was emphasized how this feature was not found in YVO. The feature disappeared upon cooling from room temperature to 100 K, and it was assigned to a biorbiton based on its high excitation energy [58]. $LaTiO_3$ and $YTiO_3$ have also been studied with RIXS at the Ti L_3 edge, and broad peaks attributed to orbital excitations were observed at an energy loss of slightly less than 300 meV [75,91]. Large intensity variations were observed between room temperature and 20 K in an experiment performed with comparable resolution but in linear horizontal polarization [91]. In this case, the excitations did not exhibit such clear energy shifts as observed here, and only a 10 meV shift can be deduced by visual inspection; hence, our data pinpoint an interesting distinction between the vanadate and titanate compounds.

D. Crystal field theory calculations

Crystal field multiplet calculations were performed using the QUANTY [92] package in order to interpret our results in a local picture. The simulations were done assuming a V $3d^2$ ion. The model Hamiltonian included the crystal field term, valence and core-valence spin-orbit interaction, and the valence and core-valence Coulomb interaction. The matrix elements of the Coulomb interaction and the spin-orbit coupling constants were taken from atomic Hartree-Fock calculations [93].

The adjustable parameters of the model in D_{4h} symmetry are the screening of the Coulomb interaction β; the octahedral component of the crystal field splitting Dq; and Ds and Dt, which describe the distortion of the octahedron and the resulting intra-t_{2g}/e_g splitting [73]. We also chose to use the same β for the core-valence and valence Coulomb interaction. The temperature dependence of the spectra was simulated by using the Boltzmann distribution to calculate the statistical weights of the low-energy eigenstates of the Hamiltonian. The weights were then used to calculate the spectrum as an average over the thermally populated initial electronic configurations.

By comparison with the experimental XAS in Fig. 2(a), it was found that $\beta = 0.65$ and $Dq = 0.21$ eV do a good job in reproducing the overall line shape, and also the energy separation of peaks A–C. We found that the absorption spectrum was not very sensitive to the crystal field parameters Dt and Ds. To determine them, we made the assumption that the RIXS peak **c** reflects the splitting of the t_{2g} single-particle orbitals into the e_g and b_{2g} orbitals. The splitting of the single-particle states $\Delta E_{t_{2g}} = E_{e_g} - E_{b_{2g}} = 3Ds - 5Dt$ was fixed to 160 meV. We then varied the e_g orbital splitting $\Delta E_{e_g} = E_{b_{1g}} - E_{a_{1g}} = 4Ds + 5Dt$ under the constraint $3Ds - 5Dt = 160$ meV, computed RIXS spectra, and compared the results to experiment in Fig. 2(c). We found that $Ds = -0.037$ eV and $Dt = 0.009$ eV give a good account of the RIXS spectra. During the comparisons, it was also found that only small values $|Ds| < 50$ meV and $|Dt| < 50$ meV of the distortion parameters resulted in a line shape in qualitative agreement with experiment. We show these results for incident energies corresponding to features A and B of Fig. 2(a) in Figs. 4(a) and 4(b), respectively. The good agreement verifies that the distortion of the octahedron in LVO is, indeed, quite small, and it is in line with results of LDA+DMFT calculations on the crystal field levels of LVO and with structural data [12,20]. The LDA+DMFT calculations were performed for the bulk monoclinic structure, and the V(1) site was found to have intra-t_{2g} crystal field splittings of 50 and approximately 150 meV, and the V(2) site had 50 and approximatively 200 meV.

We present the obtained states of the $3d^2$ configuration up to 3.4 eV from the ground state term in Table I. The first states are $S = 1$, and they are associated with the O_h $^3T_1$ ground state term that is split into ^3E and $^3A_2$ in D_{4h}, with the former being the ground state [72]. The $^3A_2$ term is the source of the low-energy peak in the crystal field model. The next terms are $S = 0$ states $^1T_2$, ^1E, $^1B_1$, and $^1B_2$, of which the two former correspond to the low-energy side and the two latter correspond to the high-energy side of the double peak observed in the experiment between 1.1 and 1.3 eV. This peak was assigned using the O_h irreducible representations in Ref. [18], but this simplification hides the fact that one may, in fact, estimate the magnitude of the intra-t_{2g} splitting by extracting the energy difference of two peaks. The O_h $^3T_2$ term is also split into components reflecting the intra-t_{2g} and e_g splitting.

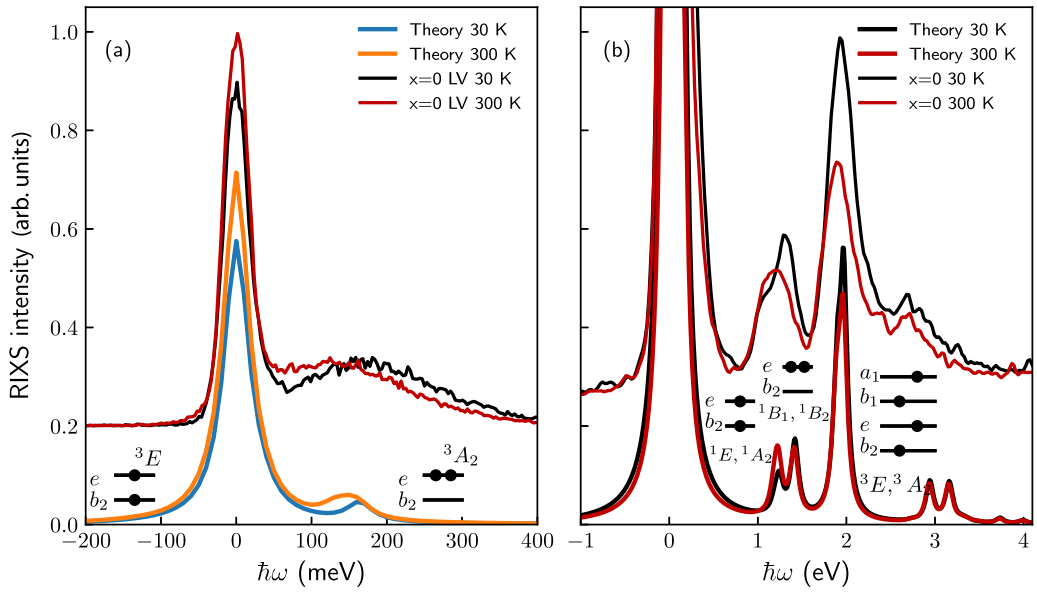

FIG. 4. (a) High-resolution experiment for LVO at 30 K vs a simulated RIXS spectrum. The incident energy was set to feature A of Fig. 2(a). Due to the domain structure of the sample, the presented spectra are averages over the appropriate linear polarization configurations. (b) RIXS simulated at feature B of Fig. 2. The energy level scheme for the $^3A_2/^3E$ peak should be understood as possible configurations of $^1t_{2g}{}^1e_g$ with $S = 1$.

It is found at approximately 2 eV above the ground state, and it is the first excited state with an $^1t_{2g}\ ^1e_g$ configuration. The assignments are in agreement with earlier works on $NdVO_3$ and YVO [18,58,72]. We have also performed calculations taking metal-ligand hybridization [92] into account. We used a charge transfer energy of 4 eV and t_{2g} (e_g) hopping of 2.08 eV (3.12 eV) derived from the literature [69]. No essential differences were found in terms of the line shape of the low- and high-energy crystal field excitations, but the Dq value had to be reduced to 0.16–0.18 eV to achieve good agreement with the energy position of the $^3A_2$ and ^3E states. The crystal field model has less adjustable parameters, and hence, we show only these results.

TABLE I. The crystal field multiplets of a $3d^2$ configuration in a D_{4h} crystal field. The listed energies correspond to the lowest spin-orbit sublevel of the configuration further characterized by the irreducible representation (Irrep). We also show the corresponding electron configuration (Config.) in the O_h nomenclature.

Energy (eV)	N_{states}	Irrep	Spin	Config.
0	6	^3E	1	$^2t_{2g}$
0.163	3	$^3A_2$	1	$^2t_{2g}$
1.205	1	$^1A_1$	0	$^2t_{2g}$
1.245	2	^1E	0	$^2t_{2g}$
1.349	2	$^1B_1, ^1B_2$	0	$^2t_{2g}$
1.796	3	$^3A_2$	1	$^1t_{2g}^1e_g$
1.861	6	^3E	1	$^1t_{2g}^1e_g$
2.725	1	$^1A_1$	0	$^2t_{2g}$
2.830	3	$^3B_2$	1	$^1t_{2g}{}^1e_g$
3.061	6	^3E	1	$^1t_{2g}^1e_g$
3.207	1	$^1A_2$	0	$^1t_{2g}^1e_g$
3.273	3	^1E	0	$^1t_{2g}^1e_g$

E. On the RIXS line shape at the V L_3 edge and the origin of the temperature effect

The crystal field model presented in the previous section performed well in reproducing the energies of the high-energy crystal field excitations and was able to describe qualitatively the temperature dependence of their intensities. Furthermore, the model can also qualitatively describe the gap closing effect seen at **b**. It, however, fails in reproducing the evolution of the spectra at the high-energy edge of **c**, and the intensity past 200 meV is naturally not reproduced as the intra-t_{2g} splitting sets the highest excitation energy scale in the vicinity of the elastic line. Furthermore, had we used, e.g., D_{3h} symmetry to fully split the t_{2g} states along the lines of the previously cited LDA+DMFT results, the added excitations would have contributed less than 100 meV energy losses [12]. The high-energy continuum was attributed to biorbitons and multiphonon excitations for YVO [18].

Structural data for bulk LVO show that the V-O bonds contract by less than 0.4% upon cooling from room temperature to 150 K. Upon cooling further to 10 K, two of the bonds contract by 2.5%, and one contracts by 1% [20]. The O ions are the dominant contribution to the crystal field potential, and the accelerated evolution of the V-O distances below the OO/AFM transition is consistent with our results. Structural properties of LVO films on STO substrates have been studied with diffraction techniques [27,33,35,36]. The temperature dependence of the out-of-plane lattice parameter ([110] of the bulk *Pnma* structure) was studied using laboratory-based x-ray diffraction, and it was found to remain constant between 300 and 10 K [36]. The in-plane lattice parameters are expected to follow the thermal contraction of the substrate, which reduces from 3.92 to 3.91 Å between 300 and 150 K and remains constant from thereon [36]. This in contrast to

the behavior of bulk LVO, where the lattice parameters evolve more rapidly below the OO/AFM transition.

The epitaxial constraint must certainly force the lattice to relax in a distinct fashion with respect to the bulk system when entering the ordered phase. Unfortunately, refined structures of LVO on STO near and below the OO/AFM transition have not been published to our knowledge. It is plausible that the structural distortions associated with the OO and AFM transitions require high-resolution diffraction or extended x-ray absorption fine-structure studies to be observed. Comparing our case to bulk YVO, which evolves structurally similarly to bulk LVO between 300 and 100 K, a blueshift of a similar magnitude was observed between 300 and 100 K [17,18], This constrains the role of the lattice distortion in the blueshift to at least mimic the bulk behavior. We note that a recent resonant photoemission study of LVO on $LaAlO_3$ (corresponding to compressive strain in contrast to the tensile strain in the case of STO) found temperature-dependent features in the O-dominated part of the valence band and interpreted the results via differences in hybridization induced by the structural phase transition found in bulk LVO [94]. Direct observations of the structural phase transition in LVO/LSVO films are lacking, but as the hybridization determines the splitting of the t_{2g} states [12,76] our observation of the blueshift is consistent with the conclusion of Jana *et al.* [94].

Raman scattering studies on LVO and $PrVO_3$ thin films have found that phonon modes associated with the bulk orbital ordering transition become active around 140 K in thin films as well [39,40]. For $PrVO_3$ thin films, the antiferromagnetic transition has been observed, and the critical temperature was observed to be reduced by 80 K from the bulk value, whereas for LVO T_c does not appear to change [37,38]. Here, the curves presented in Fig. 3(d) start their upturns near the bulk OO/Néel transition critical temperatures, but change is rather gradual. Coupling of the crystal field excitations to magnons and phonons can also have an effect. Magnon coupling has been studied from the orbital superexchange perspective, from which it was found that an orbiton excitation would redshift upon entering the AFM phase for $\mathbf{q}$ along the ΓX direction and would redshift near Γ and Z and would remain unchanged at the midpoint [95]. Assuming an orbital superexchange parameter of 40 meV following Ref. [18], the model predicts a redshift of 10–20 meV. Our data show no evidence for a redshifting low-energy excitation when entering the AFM phase. $LaTiO_3$ and $YTiO_3$ have magnetic properties similar to the corresponding vanadates, but in their case the shift between room temperature and the AFM/OO phase is of the order of 10 meV. However, for $LaTiO_3$ and $YTiO_3$ the Ti-O bonds change by a few parts per thousand between room temperature and 10 K, whereas LVO and YVO exhibit changes of the order of 1%.

Hence, we conclude that the evolution of the crystal field splitting driven by the AFM/OO transition is the dominant contribution to the blueshifting of the low-energy excitation spectrum. It has been suggested that the orbital superexchange mechanism is active at room temperature in bulk LVO and is lost rapidly upon cooling [13]. We find that the spectral features resolved in the present RIXS experiment do not change appreciably until reaching the AFM/OO phase boundary. The momentum transfer dependence of the RIXS signal should be studied for conclusive proof.

IV. CONCLUSIONS

We have presented a RIXS study of temperature and doping evolution of low-energy excitations in LVO and LSVO. We found that intra-t_{2g} excitations below 200 meV blueshift upon entering the AFM/OO phase. We argue that the shift reflects mainly the evolution of the nearest- and next-to-nearest atomic positions about the V ions. The stability of the peak position between room temperature and the AFM/OO phase boundary signifies that the proposed orbital fluctuations are not important for determining the energy of this excitation. Our crystal field calculations provide a good account of the XAS and RIXS spectra and support a local interpretation. Furthermore, we found no clear signatures of V ions changing their valency upon light hole doping under bulk-sensitive experimental conditions, which implies that doping effects in LVO and LSVO deviate from a rigid classification into Mott-Hubbard or charge-transfer insulators. Our finding thus calls for a detailed theoretical investigation of doping effects beyond model approaches. Finally, we have shown that phonon response is responsible for the low-energy excitation spectrum observed in the O preedge region.

ACKNOWLEDGMENTS

This work has been supported by the Labex Palm (Grant No. ANR-10-LABX-0039-PALM). Carnot ESP is funded by Agence Nationale de la Recherche. We acknowledge Synchrotron SOLEIL and the ESRF for providing synchrotron radiation and technical support.

[1] M.-H. Sage, Ph.D. thesis, University of Groningen, 2006.
[2] S. Miyasaka, Y. Okimoto, M. Iwama, and Y. Tokura, Phys. Rev. B **68**, 100406(R) (2003).
[3] T. Mizokawa and A. Fujimori, Phys. Rev. B **54**, 5368 (1996).
[4] H. Sawada, N. Hamada, K. Terakura, and T. Asada, Phys. Rev. B **53**, 12742 (1996).
[5] T. Mizokawa, D. I. Khomskii, and G. A. Sawatzky, Phys. Rev. B **60**, 7309 (1999).
[6] G. Khaliullin, P. Horsch, and A. M. Oleś, Phys. Rev. Lett. **86**, 3879 (2001).
[7] Y. Motome, H. Seo, Z. Fang, and N. Nagaosa, Phys. Rev. Lett. **90**, 146602 (2003).
[8] Y. Ren, A. A. Nugroho, A. A. Menovsky, J. Strempfer, U. Rütt, F. Iga, T. Takabatake, and C. W. Kimball, Phys. Rev. B **67**, 014107 (2003).
[9] C. Ulrich, G. Khaliullin, J. Sirker, M. Reehuis, M. Ohl, S. Miyasaka, Y. Tokura, and B. Keimer, Phys. Rev. Lett. **91**, 257202 (2003).
[10] Z. Fang and N. Nagaosa, Phys. Rev. Lett. **93**, 176404 (2004).

[11] S. Miyasaka, S. Onoda, Y. Okimoto, J. Fujioka, M. Iwama, N. Nagaosa, and Y. Tokura, Phys. Rev. Lett. **94**, 076405 (2005).

[12] I. V. Solovyev, Phys. Rev. B **74**, 054412 (2006).

[13] M. De Raychaudhury, E. Pavarini, and O. K. Andersen, Phys. Rev. Lett. **99**, 126402 (2007).

[14] P. Horsch, A. M. Oleś, L. F. Feiner, and G. Khaliullin, Phys. Rev. Lett. **100**, 167205 (2008).

[15] J.-S. Zhou, Y. Ren, J.-Q. Yan, J. F. Mitchell, and J. B. Goodenough, Phys. Rev. Lett. **100**, 046401 (2008).

[16] K. Rościszewski and A. M. Oleś, Phys. Rev. B **98**, 085119 (2018).

[17] G. R. Blake, T. T. M. Palstra, Y. Ren, A. A. Nugroho, and A. A. Menovsky, Phys. Rev. B **65**, 174112 (2002).

[18] E. Benckiser, L. Fels, G. Ghiringhelli, M. Moretti Sala, T. Schmitt, J. Schlappa, V. N. Strocov, N. Mufti, G. R. Blake, A. A. Nugroho, T. T. M. Palstra, M. W. Haverkort, K. Wohlfeld, and M. Grüninger, Phys. Rev. B **88**, 205115 (2013).

[19] J. Reul, A. A. Nugroho, T. T. M. Palstra, and M. Grüninger, Phys. Rev. B **86**, 125128 (2012).

[20] P. Bordet, C. Chaillout, M. Marezio, Q. Huang, A. Santoro, S.-W. Cheong, H. Takagi, C. Oglesby, and B. Batlogg, J. Solid State Chem. **106**, 253 (1993).

[21] G. Sclauzero and C. Ederer, Phys. Rev. B **92**, 235112 (2015).

[22] G. Sclauzero, K. Dymkowski, and C. Ederer, Phys. Rev. B **94**, 245109 (2016).

[23] C. He, T. D. Sanders, M. T. Gray, F. J. Wong, V. V. Mehta, and Y. Suzuki, Phys. Rev. B **86**, 081401(R) (2012).

[24] H. Weng and K. Terakura, Phys. Rev. B **82**, 115105 (2010).

[25] Y. Hotta, T. Susaki, and H. Y. Hwang, Phys. Rev. Lett. **99**, 236805 (2007).

[26] A. Jana, R. J. Choudhary, and D. M. Phase, Phys. Rev. B **98**, 075124 (2018).

[27] H. Rotella, O. Copie, G. Steciuk, H. Ouerdane, P. Boullay, P. Roussel, M. Morales, A. David, A. Pautrat, B. Mercey, L. Lutterotti, D. Chateigner, and W. Prellier, J. Phys.: Condens. Matter **27**, 175001 (2015).

[28] F. Inaba, T. Arima, T. Ishikawa, T. Katsufuji, and Y. Tokura, Phys. Rev. B **52**, R2221 (1995).

[29] S. Miyasaka, T. Okuda, and Y. Tokura, Phys. Rev. Lett. **85**, 5388 (2000).

[30] H. C. Nguyen and J. B. Goodenough, Phys. Rev. B **52**, 324 (1995).

[31] L. D. Tung, A. Ivanov, J. Schefer, M. R. Lees, G. Balakrishnan, and D. M. Paul, Phys. Rev. B **78**, 054416 (2008).

[32] R. Khan, J. Bashir, N. Iqbal, and M. Khan, Mater. Lett. **58**, 1737 (2004).

[33] H. Rotella, U. Lüders, P.-E. Janolin, V. H. Dao, D. Chateigner, R. Feyerherm, E. Dudzik, and W. Prellier, Phys. Rev. B **85**, 184101 (2012).

[34] Y. Hotta, Y. Mukunoki, T. Susaki, H. Y. Hwang, L. Fitting, and D. A. Muller, Appl. Phys. Lett. **89**, 031918 (2006).

[35] I. C. Lekshmi, A. Gayen, and M. Hegde, J. Phys. Chem. Solids **66**, 1647 (2005).

[36] H. Meley, Karandeep, L. Oberson, J. de Bruijckere, D. T. L. Alexander, J.-M. Triscone, P. Ghosez, and S. Gariglio, APL Mater. **6**, 046102 (2018).

[37] O. Copie, H. Rotella, P. Boullay, M. Morales, A. Pautrat, P.-E. Janolin, I. C. Infante, D. Pravathana, U. Lüders, and W. Prellier, J. Phys.: Condens. Matter **25**, 492201 (2013).

[38] L. Wang, Y. Li, A. Bera, C. Ma, F. Jin, K. Yuan, W. Yin, A. David, W. Chen, W. Wu, W. Prellier, S. Wei, and T. Wu, Phys. Rev. Appl. **3**, 064015 (2015).

[39] I. Vrejoiu, C. Himcinschi, L. Jin, C.-L. Jia, N. Raab, J. Engelmayer, R. Waser, R. Dittmann, and P. H. M. van Loosdrecht, APL Mater. **4**, 046103 (2016).

[40] I. Lindfors-Vrejoiu, L. Jin, C. Himcinschi, J. Engelmayer, F. Hensling, C.-L. Jia, R. Waser, R. Dittmann, and P. H. M. Loosdrecht, Phys. Status Solidi RRL **11**, 1600350 (2017).

[41] H. Meley, M. Tran, J. Teyssier, J. A. Krieger, T. Prokscha, A. Suter, Z. Salman, M. Viret, D. van der Marel, and S. Gariglio, Phys. Rev. B **103**, 125112 (2021).

[42] N. F. Mott, *Metal-Insulator Transitions*, 2nd ed. (Taylor and Francis, London, 1990).

[43] M. Imada, A. Fujimori, and Y. Tokura, Rev. Mod. Phys. **70**, 1039 (1998).

[44] A. Fujimori, T. Yoshida, K. Okazaki, T. Tsujioka, K. Kobayashi, T. Mizokawa, M. Onoda, T. Katsufuji, Y. Taguchi, and Y. Tokura, J. Electron Spectrosc. Relat. Phenom. **117–118**, 277 (2001).

[45] K. Maiti and D. D. Sarma, Phys. Rev. B **61**, 2525 (2000).

[46] J. Zaanen, G. A. Sawatzky, and J. W. Allen, Phys. Rev. Lett. **55**, 418 (1985).

[47] A. V. Mahajan, D. C. Johnston, D. R. Torgeson, and F. Borsa, Phys. Rev. B **46**, 10973 (1992).

[48] J. Fujioka, S. Miyasaka, and Y. Tokura, Phys. Rev. Lett. **97**, 196401 (2006).

[49] R. Egdell, M. Harrison, M. Hill, L. Porte, and G. Wall, J. Phys. C **17**, 2889 (1984).

[50] S. Miyasaka, Y. Okimoto, and Y. Tokura, J. Phys. Soc. Jpn **71**, 2086 (2002).

[51] Z. Fang, N. Nagaosa, and K. Terakura, Phys. Rev. B **67**, 035101 (2003).

[52] M. Kim, Phys. Rev. B **97**, 155141 (2018).

[53] L. J. P. Ament, M. van Veenendaal, T. P. Devereaux, J. P. Hill, and J. van den Brink, Rev. Mod. Phys. **83**, 705 (2011).

[54] N. Brookes, F. Yakhou-Harris, K. Kummer, A. Fondacaro, J. Cezar, D. Betto, E. Velez-Fort, A. Amorese, G. Ghiringhelli, L. Braicovich, R. Barrett, G. Berruyer, F. Cianciosi, L. Eybert, P. Marion, P. van der Linden, and L. Zhang, Nucl. Instrum. Methods Phys. Res., Sect. A **903**, 175 (2018).

[55] A. Amorese, N. Caroca-Canales, S. Seiro, C. Krellner, G. Ghiringhelli, N. B. Brookes, D. V. Vyalikh, C. Geibel, and K. Kummer, Phys. Rev. B **97**, 245130 (2018).

[56] A. Amorese, O. Stockert, K. Kummer, N. B. Brookes, D.-J. Kim, Z. Fisk, M. W. Haverkort, P. Thalmeier, L. H. Tjeng, and A. Severing, Phys. Rev. B **100**, 241107(R) (2019).

[57] B. Chen, J. Laverock, D. Newby, Jr., J. F. McNulty, K. E. Smith, P.-A. Glans, J.-H. Guo, R.-M. Qiao, W.-L. Yang, M. R. Lees, L. D. Tung, R. P. Singh, and G. Balakrishnan, J. Phys.: Condens. Matter **27**, 105503 (2015).

[58] J. Laverock, B. Chen, A. R. H. Preston, D. Newby Jr., L. F. J. Piper, L. D. Tung, G. Balakrishnan, P.-A. Glans, J.-H. Guo, and K. E. Smith, J. Phys.: Condens. Matter **26**, 455603 (2014).

[59] M. Sacchi, N. Jaouen, H. Popescu, R. Gaudemer, J. M. Tonnerre, S. G. Chiuzbaian, C. F. Hague, A. Delmotte, J. M. Dubuisson, G. Cauchon, B. Lagarde, and F. Polack, J. Phys.: Conf. Ser. **425**, 072018 (2013).

[60] S. G. Chiuzbăian, C. F. Hague, A. Avila, R. Delaunay, N. Jaouen, M. Sacchi, F. Polack, M. Thomasset, B. Lagarde, A.

Nicolaou, S. Brignolo, C. Baumier, J. Lüning, and J.-M. Mariot, Rev. Sci. Instrum. **85**, 043108 (2014).
[61] L. J. P. Ament, M. van Veenendaal, and J. van den Brink, Europhys. Lett. **95**, 27008 (2011).
[62] H.-T. Zhang, M. Brahlek, X. Ji, S. Lei, J. Lapano, J. W. Freeland, V. Gopalan, and R. Engel-Herbert, ACS Appl. Mater. Interfaces **9**, 12556 (2017).
[63] H. Wadati, D. G. Hawthorn, J. Geck, T. Z. Regier, R. I. R. Blyth, T. Higuchi, Y. Hotta, Y. Hikita, H. Y. Hwang, and G. A. Sawatzky, Appl. Phys. Lett. **95**, 023115 (2009).
[64] H. F. Pen, M. Abbate, A. Fujimori, Y. Tokura, H. Eisaki, S. Uchida, and G. A. Sawatzky, Phys. Rev. B **59**, 7422 (1999).
[65] J.-H. Park, L. H. Tjeng, A. Tanaka, J. W. Allen, C. T. Chen, P. Metcalf, J. M. Honig, F. M. F. de Groot, and G. A. Sawatzky, Phys. Rev. B **61**, 11506 (2000).
[66] T. Schmitt, L.-C. Duda, A. Augustsson, J.-H. Guo, J. Nordgren, J. E. Downes, C. McGuinness, K. E. Smith, G. Dhalenne, A. Revcolevschi, M. Klemm, and S. Horn, Surf. Rev. Lett. **09**, 1369 (2002).
[67] M. W. Haverkort, Z. Hu, A. Tanaka, W. Reichelt, S. V. Streltsov, M. A. Korotin, V. I. Anisimov, H. H. Hsieh, H.-J. Lin, C. T. Chen, D. I. Khomskii, and L. H. Tjeng, Phys. Rev. Lett. **95**, 196404 (2005).
[68] H. Wadati, Ph.D. thesis, University of Tokyo, 2006.
[69] R. J. O. Mossanek, M. Abbate, P. T. Fonseca, A. Fujimori, H. Eisaki, S. Uchida, and Y. Tokura, Phys. Rev. B **80**, 195107 (2009).
[70] C. T. Chen, F. Sette, Y. Ma, M. S. Hybertsen, E. B. Stechel, W. M. C. Foulkes, M. Schluter, S.-W. Cheong, A. S. Cooper, L. W. Rupp, B. Batlogg, Y. L. Soo, Z. H. Ming, A. Krol, and Y. H. Kao, Phys. Rev. Lett. **66**, 104 (1991).
[71] J. van Elp, H. Eskes, P. Kuiper, and G. A. Sawatzky, Phys. Rev. B **45**, 1612 (1992).
[72] V. Yushankhai and L. Siurakshina, Int. J. Mod. Phys. B **27**, 1350185 (2013).
[73] F. De Groot and A. Kotani, *Core Level Spectroscopy of Solids*, Advances in Condensed Matter Science (Taylor and Francis, Boca Raton, 2008).
[74] N. A. Bogdanov, J. van den Brink, and L. Hozoi, Phys. Rev. B **84**, 235146 (2011).
[75] C. Ulrich, G. Ghiringhelli, A. Piazzalunga, L. Braicovich, N. B. Brookes, H. Roth, T. Lorenz, and B. Keimer, Phys. Rev. B **77**, 113102 (2008).
[76] E. Pavarini, A. Yamasaki, J. Nuss, and O. K. Andersen, New J. Phys. **7**, 188 (2005).
[77] K. Haule, T. Birol, and G. Kotliar, Phys. Rev. B **90**, 075136 (2014).
[78] A. Geondzhian and K. Gilmore, Phys. Rev. B **98**, 214305 (2018).
[79] A. Geondzhian and K. Gilmore, Phys. Rev. B **101**, 214307 (2020).
[80] N. Choudhury, E. J. Walter, A. I. Kolesnikov, and C.-K. Loong, Phys. Rev. B **77**, 134111 (2008).
[81] V. Vaz da Cruz, F. Gel'mukhanov, S. Eckert, M. Iannuzzi, E. Ertan, A. Pietzsch, R. C. Couto, J. Niskanen, M. Fondell, M. Dantz, T. Schmitt, X. Lu, D. McNally, R. M. Jay, V. Kimberg, A. Föhlisch, and M. Odelius, Nat. Commun. **10**, 1013 (2019).
[82] J. Fujioka, S. Miyasaka, and Y. Tokura, Phys. Rev. B **77**, 144402 (2008).
[83] Y.-P. Sun, F. Hennies, A. Pietzsch, B. Kennedy, T. Schmitt, V. N. Strocov, J. Andersson, M. Berglund, J.-E. Rubensson, K. Aidas, F. Gel'mukhanov, M. Odelius, and A. Föhlisch, Phys. Rev. B **84**, 132202 (2011).
[84] F. Hennies, A. Pietzsch, M. Berglund, A. Föhlisch, T. Schmitt, V. Strocov, H. O. Karlsson, J. Andersson, and J.-E. Rubensson, Phys. Rev. Lett. **104**, 193002 (2010).
[85] V. Ilakovac, S. Carniato, P. Foury-Leylekian, S. Tomić, J.-P. Pouget, P. Lazić, Y. Joly, K. Miyagawa, K. Kanoda, and A. Nicolaou, Phys. Rev. B **96**, 184303 (2017).
[86] C. Monney, V. Bisogni, K.-J. Zhou, R. Kraus, V. N. Strocov, G. Behr, J. Málek, R. Kuzian, S.-L. Drechsler, S. Johnston, A. Revcolevschi, B. Büchner, H. M. Rønnow, J. van den Brink, J. Geck, and T. Schmitt, Phys. Rev. Lett. **110**, 087403 (2013).
[87] E. Ertan, V. Kimberg, F. Gel'mukhanov, F. Hennies, J.-E. Rubensson, T. Schmitt, V. N. Strocov, K. Zhou, M. Iannuzzi, A. Föhlisch, M. Odelius, and A. Pietzsch, Phys. Rev. B **95**, 144301 (2017).
[88] K. Habicht, D. Wong, and C. Schulz (private communication).
[89] A. Avella, A. M. Oleś, and P. Horsch, Phys. Rev. B **97**, 155104 (2018).
[90] S. Miyasaka, J. Fujioka, M. Iwama, Y. Okimoto, and Y. Tokura, Phys. Rev. B **73**, 224436 (2006).
[91] C. Ulrich, L. J. P. Ament, G. Ghiringhelli, L. Braicovich, M. M. Sala, N. Pezzotta, T. Schmitt, G. Khaliullin, J. van den Brink, H. Roth, T. Lorenz, and B. Keimer, Phys. Rev. Lett. **103**, 107205 (2009).
[92] M. W. Haverkort, M. Zwierzycki, and O. K. Andersen, Phys. Rev. B **85**, 165113 (2012).
[93] M. Haverkort, Ph.D. thesis, University of Cologne, 2004.
[94] A. Jana, R. Raghunathan, R. Rawat, R. J. Choudhary, and D. M. Phase, Phys. Rev. B **102**, 235108 (2020).
[95] S. Ishihara, Phys. Rev. B **69**, 075118 (2004).